[1]Contribution of microstructural parameters to strengthening in an ultrafine-grained Al-7%Si alloy processed by severe deformation

I. Gutierrez-Urrutia, M.A. Muñoz-Morris and D.G. Morris
Department of Physical Metallurgy, CENIM, CSIC, Avenida Gregorio del Amo 8, 28035 Madrid, SPAIN

Abstract

An Al-7%Si alloy was severely deformed by equal channel angular pressing (ECAP) to study the refinement of the microstructure and associated changes of mechanical properties. The initial coarse dendritic structure was broken into an elongated sub-micron grain/subgrain structure, with high dislocation density, and distributed fine Si particles. The Si particles in the composite are seen to induce a high dislocation density during deformation and lead to faster structural refinement than in a monolithic alloy with the same composition as the matrix. The additional strengthening of the composite relative to the monolithic alloy is due to both the finer grain size and the high retained dislocation density. Severe plastic deformation leads also to an improvement of the ductility of the strong material due to the refinement of both matrix microstructure and the Si particles.

Keywords
Equal Channel Angular Pressing (ECAP); Mechanical properties; Nanostructures; Annealing

Introduction

Al-Si alloys are widely used because of their low density, good castability and high strength at elevated temperatures. They suffer, however, from low ductility or toughness, which limits their use to applications where these properties are not important. There has been a continuous effort over the past years to enhance mechanical properties by changing solidification conditions, additional heat treatments, or introducing alloying elements to modify Si particle morphology [1].

Modifications of microstructure are also possible by severe plastic deformation, for example by ECAP, which has been extensively studied on single phase metals and alloys [2-10]. Structural refinement by the creation of intense dislocation substructures has been well documented, as well as the improvement in strength that is achieved. The role of second phase particles during severe plastic deformation has been much less examined, although some studies have shown that particle shearing or even dissolution may sometimes be possible [11-16]. The role of large particles in accelerating structural refinement has been demonstrated,

[1] ***Publicado en ACTA MATERIALIA 55, 1319-1330 (2007); DOI: 10.1016/j.actamat.2006.09.037***

based on the formation of large strain and misorientation gradients in the matrix close to these particles [17-19].

A small amount of work has been reported on the influence of severe plastic deformation, by a rotary-die ECAP method, on Al-Si alloys containing large amounts of Si (typically 11-23 wt%Si) [20-23]. This work has shown that it is possible to refine the size of the Si particles, from tens of microns typical of the as-cast state to several microns, by severe deformation, and this leads to a large improvement in ductility, toughness, and wear resistance. Surprisingly little strengthening was, however, reported in such studies, despite some refinement of grain size as well as of the Si particles present.

The present study sets out to follow in detail the microstructure evolution, both Si particle refinement as well as structural changes in the Al matrix, during the severe plastic deformation by ECAP of a hypoeutectic Al-7wt%Si alloy. Changes in mechanical behaviour observed after severe plastic deformation are examined in terms of the microstructure evolution taking account of changes to the matrix (dislocations and boundaries) as well as changes to the Si particle distribution.

Experimental Details

A hypoeutectic Al-7%Si (weight percent is used throughout, unless specifically indicated otherwise) alloy was prepared from commercially pure Al and Si, melting under protective atmosphere and casting into bars of 35 mm diameter. Bars of commercially pure Al and of Al-0.5%Si were also cast as reference materials. The alloy with 0.5%Si was chosen as the same composition as the matrix in the Al-7%Si composite once Si particles separated out during solidification, to evaluate the behaviour of the matrix in the absence of such particles. These bars were machined into cylinders 20 mm in diameter and 60 mm long for ECAP processing at room temperature. ECAP was carried out by pressing through a die with angle of 118-120º, producing a true strain of 0.7. Details of processing conditions are given elsewhere [7]. Repeated pressing used the so-called route A [3, 4], whereby there is no rotation of sample between passes. Samples were processed, at room temperature, up to ten passes, corresponding to a total strain of 7.

Microstructures were examined by scanning electron microscopy (SEM) using a JEOL 6500FX instrument and by transmission electron microscopy (TEM) using a JEOL 2010 instrument. Polished sections and thin foil samples were prepared by electropolishing using 5% perchloric acid in methanol at 0ºC and 20V. The longitudinal section was examined, i.e. the observation direction was perpendicular to the inlet and outlet ECAP cylinder axes such that the extent of microstructural elongation was clearly visible [7].

Quantitative image analysis was carried out to measure the evolution of Si particle size and matrix grain size during successive ECAP passes. For the statistical measurements of grain size (grain width and length) between 500 and 1000 grains were measured from SEM images obtained using back-scattered electrons and electron channeling contrast. From the histograms obtained, the median value (defined as that where 50% of the grains were larger and smaller) was taken for the corresponding width and length of the grains. This procedure was also used for the measurements of the Si particles, measuring at least 500 particles in each case. Measurements of dislocation density inside the boundaries of heavily deformed samples were also made on typical transmission electron micrographs, imaging generally in bright field, and estimating foil thickness from the identified diffraction vector and counting the number of fringes at the boundaries.

For evaluation of mechanical properties of the cast and severely deformed samples, tensile and compression testing was performed, using a universal testing machine at a strain rate of 4 x 10^{-4} s^{-1}. For the compression tests, cylinders 3 mm in diameter and 5 mm in height were used and samples were taken such that the compression axis was the same as the observation direction of microstructural examination. The tensile samples were also cylindrical, with gauges of 3 mm diameter and 20 mm length, that were machined with the tensile axis perpendicular to the observation direction, and along the ECAP sample axis direction (i.e inlet and outlet direction). At least three samples were tested in each case.

Results

Microstructural evolution during severe deformation

The as-cast Al-7%Si exhibited a typical hypoeutectic solidification structure, consisting of primary aluminium dendrites and interdendritic networks of lamellar eutectic silicon (see Fig. 1a). Fe impurities in the alloy led to the formation of a small amount (less than 0.5% by volume) of β-(Al_5FeSi) particles. The dendrite arms defined solidification cells of size about 25 μm, with Si particles, average size 3.8 μm wide and 6.2 μm long, present in the interdendritic region with a volume fraction of 9%. Fig. 1 shows the general morphology of these interdendritic networks, that became elongated with increasing deformation as the Si particles are broken and somewhat distributed. The initial as-cast interdendritic network, Fig. 1a, changed into a banded structure (15 μm wide-100 μm long) of finer particles (1.9 μm wide-4.8 μm long) after two ECAP passes, Fig. 1b, with further narrowing and elongation of these bands with continued deformation. The Si particles continued to refine in size at larger strains, and were more homogeneously distributed within the banded regions as shown in Fig. 1c-1d. Higher magnification images showing details of the Si particles are shown in Fig.1e-1f

for as-cast material and after ten ECAP passes respectively, while the average particle sizes measured are given in Table 1.

Matrix grain microstructures after severe deformation of the Al-7%Si alloy are illustrated in the SEM images of Fig. 2, obtained by crystallographic contrast using backscattered electrons, with average values of grain/subgrain size, width and length, listed in Table 1. Fig. 2a illustrates an example of the microstructure after one ECAP pass, where the initial 500 μm coarse grains of the as-cast material were rapidly subdivided by shear bands, about 4-5 μm apart, produced at the beginning of deformation. Within these bands, a large proportion of the material (about 60%) was subdivided into elongated subgrains 420 nm width and length ranging between 800-1500 nm. At this stage of deformation it is clear that the microstructure is relatively inhomogeneous, containing regions of more or less defined dislocation cells, subgrains and deformation bands. With further ECAP passes grain /subgrain refinement inside the bands continued, the microstructure became more homogeneous, and the crystallographic contrast increased substantially, as illustrated in Fig. 2b after four ECAP passes. This subgrain/grain contrast became more pronounced after eight and ten passes revealing very clearly a homogeneous distribution of fine but still elongated grains, as shown in Figs. 2c and 2d, where grain sizes of 200 - 170 nm width and 520 - 420 nm length have been measured. Corresponding microstructures observed by TEM provided information on the initial subgrain formation, separated by low angle boundaries, after one ECAP pass, Fig. 3a. After four ECAP passes, see Fig. 3b, some increase in dislocation density was noted within the subgrain interiors, while the increase in misorientation across individual grains/subgrains boundaries is confirmed, by examination of Kikuchi patterns and diffraction spot patterns, to be responsible for the increase in crystallographic contrast observed in the SEM images. Fig.3c shows the grains observed after ten ECAP passes, which now have a smaller width and length than after smaller amounts of strain. This is also seen in Table 1 where we note that the most important change observed with increasing strain was the decrease of both width and length of the grains, rapidly for the initial strains and more slowly at higher strain levels; the grain aspect ratio (length divided by width) remains relatively constant. It may also be noted in Fig. 3 that the dislocations inside the subgrains/grains show some tendency to arrange as loose cell walls, but are generally rather uniformly and randomly distributed.

During the initial stages of deformation, there is an increase in the density of boundaries of low misorientation, with more-widely separated intense boundaries (at microbands or heavy dislocation walls) subdividing the initial large grains into small regions. At higher strains the density of the intense boundaries approaches that of the lower misorientation boundaries, and so the grain size reduces close to the level of the cell boundaries, which become sparser inside

the grains. This general description of microstructure evolution during heavy deformation [23,24] is consistent with the evolution of the histograms of grain size (length or width), as shown in Fig. 4: after small amounts of strain the boundary distribution is more inhomogeneous, with many low misorientation and few high misorientation boundaries, giving rise to a wide histogram of sizes; after progressively higher amounts of strain the boundary distribution becomes narrower as cell boundary spacing approaches that of the higher angle grain boundaries, and the histogram tail at large grain size fades away.

TEM observations of the severely deformed microstructures, see Fig.5, provided additional information on the effect of the coarse Si particles on grain refinement. Small, equiaxed grains, characteristic of dynamic recrystallization, were seen to have formed in zones adjacent to the coarse Si particles, as shown in Fig.5 after eight ECAP passes. The size of these grains was already very small after two ECAP passes (180 nm, measured from TEM images) and remained rather constant after straining further, to eight and ten passes. Such well-defined equiaxed grains were produced close around the Si particles, even though the bulk of the Al matrix had much more poorly defined and elongated grain structures, as described earlier (Fig. 3).

The evolution of grain size during ECAP was also measured for the aluminium and the Al-0.5%Si alloy to obtain information on the influence of Si in solution and as dispersed second phase particles on grain size reduction during severe deformation. Fig 6 shows examples of microstructures in these materials after one, four and eight ECAP passes. It is again clear here that the microstructure is less clearly defined and more inhomogeneous after one ECAP pass, showing intermixed regions of well-defined subgrains/shear bands and regions of weak cellular contrast, and higher strain levels are required to obtain the uniform elongated subgrain/grain microstructure. Even after the highest imposed strain the grain size achieved in the Al-0.5%Si alloy remains much larger (290 nm width) than that measured in the Al-7%Si material (170nm width) and similar to that of the heavily deformed aluminium (see Table 2). Figure 7 shows TEM micrographs comparing the grain size and internal dislocation density in samples of the Al-0.5%Si and Al-7%Si after deforming to eight ECAP passes. It is clear that the grain size is much larger in the Al-0.5%Si alloy, and the dislocation density retained inside these grains is much lower, than in the alloy with high silicon content.

Mechanical testing results

The severe deformation process produced an important increase in the mechanical strength of the materials, not only in the Al-7%Si alloy, but also in the Al-0.5%Si alloy and in the aluminium used as reference materials. Fig. 8 gives examples of true stress – true strain tensile curves obtained on the Al-7%Si material when tested in the as cast state and after

deforming by 10 passes of ECAP, illustrating this strength increase. The measured values of the yield stress are given in Tables 1 and 2 where the most pronounced increases are confirmed to occur during the first two ECAP passes. It is worth noting that the yield stresses measured in tension and compression showed no difference, neither did they show any change when compression testing was done with the compression axis along different directions. The data scatter given in the Tables represent the dispersion of data for the three tests carried out at each state.

Fig. 9 shows the evolution of yield stress as a function of total strain by ECAP for all the materials examined. We note that, although the stresses are higher for the Al-7%Si alloy, the evolution is very similar for all three materials, that the stress increase is rapid for the first ECAP pass (and this increase is twice as high in the Al-7Si as in the Al-0.5Si), and that after a strain of 2 (three ECAP passes) there is only a small subsequent increase in stress for all materials. It is also worth noting that the stress values for the Al-0.5%Si alloy are practically the same as those obtained for the aluminium, within the few MPa of data scatter (see table 2).

A major difference in behaviour of the heavily deformed Al-7%Si compared with the as-cast state is the great increase in tensile ductility, from 4.5% in the as-cast state to 13% after severe deformation by ten ECAP passes, as seen in Fig. 8. Here, it is also seen that the heavily deformed materials are characterised by the well-known much lower work hardening than for the as-cast materials [e.g. 6,11], which generally contributes to a reduction of ductility of the severely plastically deformed materials. Images obtained by SEM of the fracture surfaces of tensile tested Al-7%Si in various states are illustrated in Fig. 10, where the role played by the finer distribution of Si particles and the finer matrix microstructure is evident. In Fig. 10a the fracture surface of the as-cast material shows a large fraction of broken Si particles and the matrix regions are relatively flat, reflecting the easy crack nucleation and propagation. In contrast, Figs. 10b and 10c show the dimpled matrix surfaces and finer broken Si particles after severe plastic deformation to a strain of 1.4 and 7. The more homogeneous, dimpled matrix fracture surfaces and finer, distributed Si particles both contribute to more difficult crack nucleation and delayed propagation, resulting in the improved ductility.

Discussion

This discussion will examine the evolution of microstructure during severe plastic deformation by ECAP, as well as examine the evolution of corresponding strength and ductility. Emphasis is placed on the analysis of the behaviour of the Al-7%Si composite alloy, containing about 9% by volume of Si particles in an Al-0.5%Si matrix, and comparison made with the behaviour of the monolithic Al-0.5%Si and Al, in order to distinguish the role played by the coarse Si particles on structure evolution and strengthening.

Microstructure evolution:

Two aspects of microstructure evolution for the Al-7%Si composite can be examined, namely the changes of Si particles and changes of Al(Si) matrix. As shown in Fig. 1 and Table 1, the as-cast structure is characterised by rather large and brittle Si particles arranged in a solidification cellular distribution between the original Al dendrites. During severe plastic deformation these coarse Si particles are broken into much finer, equiaxed particles (average size of about 4 μm initially to near 1-2 μm after very high strains, see Table 1). At the same time the general microstructure morphology changes to a layered structure of elongated Al single phase regions separated by regions of high volume fraction of broken, equiaxed Si particles interdispersed in Al matrix (such regions contain about one third by volume of Si phase and two thirds of Al, and correspond to the final solidifying eutectic). The elongated Al single phase regions gradually narrow from the initial cell size (about 25 μm) to below 10 μm after high levels of imposed strain, see Fig. 1.

Structure evolution in the Al(Si) matrix and in the monolithic Al-0.5%Si and Al materials is very similar, apart from the faster rate of structural refinement as discussed below, as is seen by comparison of Figs. 2 and 6. The evolution of deformation substructure with increasing strain has been well summarised for classical methods of deformation, for example in [24,25], as well as for severe plastic deformation by methods such as ECAP, for example in [17], and only a brief reminder is given here. During the initial stages of severe deformation (after one ECAP pass, for example, of a material such as lightly alloyed Al) the microstructure is characterised by dislocation cell blocks which are separated by heavy dislocation walls or microbands, with dislocations arranged in a cellular fashion inside the blocks. With increasing deformation, to strain levels of about 2, the cell blocks gradually refine in size to become close to the cell size as the density of heavy dislocation walls or microbands increases, and the internal dislocation structure becomes more random with less space for the cellular structures. These dislocation structures can be further understood using concepts of strain gradient plasticity [e.g. 25,26], with the cell block/microband structures forming initially due to strain gradients and the accumulation of the geometrically necessary dislocations, and the random/cellular dislocations initially forming from statistically accumulating or incidental dislocations. After the first 1-2 ECAP passes of the present study, the microstructure is still one of inhomogeneous and relatively poorly-defined cell blocks and weak cell structures inside, see Figs. 2, 3 and 6. After more severe straining as examined here, the cell blocks retain an elongated, banded structure with length approximately 2-3 times the width, as seen in Figs. 2, 3 and 6, and in Tables 1 and 2, with a high internal dislocation density, generally fairly randomly distributed. Following the initial few ECAP passes, then, the microstructure retains approximately the same morphology, of elongated single-cell blocky structures with a

high internal dislocation density, with simply a gradual decrease in the block size at higher strains, see Tables 1 and 2. While boundary misorientations are low during the initial strains, after high strains, above 2-3 passes, boundary misorientations become sufficiently high, increasing continuously at higher strain levels, that these can be regarded as subgrain/grain boundaries, and their contribution to hardening can be analysed using a Hall-Petch type of analysis [24,25]. In the analysis of subgrain/grain boundary hardening, the grain width can be reasonably taken as the more relevant size parameter [6] since it is more closely related to the dislocation pile-up or stress concentration length for dislocations interacting with the boundaries. The high density of randomly or weakly cellularly distributed dislocations, in contrast, can be considered to contribute to hardening as though these are randomly distributed, using a Taylor type approach [25]. Accurate measurements of dislocation densities from TEM photographs, such as those of Fig. 3 and Fig. 7, are difficult, whether images are taken in bright field or in weak beam conditions. Comparison of dislocation densities in Fig. 7 shows clearly the much larger dislocation density after deforming the Al-7%Si composite as compared with the Al-0.5%Si alloy. The densities are estimated to be about 1 x $10^{14}/m^2$ for the Al-7%Si composite after 4-8 ECAP passes, with little variation with strain level, and somewhat less, approximately 10^{12}-$10^{13}/m^2$, for the monolithic Al-0.5%Si alloy deformed to similar high strain levels.

The discussion above applies equally well to the monolithic Al and Al-0.5%Si as well as to the Al-7%Si materials, with the difference of a much faster structure evolution for the Al-Si composite, see Fig. 11 and compare Tables 1 and 2. Fig. 11 makes it clear that the first ECAP pass produces the greatest reduction in grain size, from the approximately 500 μm level of the as-cast materials. It should, however, be remembered that the boundaries are mostly lower-misorientation cell and cell-block boundaries at this stage of deformation, and most are not true high-angle grain boundaries. Grain size refinement continues rapidly for the first 2-3 ECAP passes (the stage that the single-cell subgrain/grain microstructure is becoming established) and thereafter continues at a slower pace, Fig. 11. Most interesting is to note, however, that grain size refinement in the Al-7Si composite is faster than in the two monolithic materials not only during the initial stages (from 500 μm to 0.42-0.3 μm by 1-2 passes as compared with refinement to 0.8-0.5 μm) but also after much higher strain levels (between 4 and 8 passes - grain size reduction greater than 15% near 0.2μm for the composite, compared with reduction less than 10% near 0.3μm for the monolithic materials). The faster structural refinement for the Si particle-containing composite can be understood in terms of the high rate of production of dislocations near the large, undeforming particles and large local strain gradients [17-19,26]. According to the strain gradient plasticity theory [26], large numbers of geometrically necessary dislocations will accumulate during straining in the matrix surrounding the large, undeformable Si particles. The density of such dislocations

(ρ_{GN}) is essentially proportional to the strain gradient, i.e. the amount of plastic strain (ε) divided by the microstructural scale (λ) over which this gradient is created ($\rho_{GN} = 8\varepsilon /3\ b\lambda$) . Here, this gradient will be proportional to the shear imposed during ECAP (strain of 0.7 per pass) divided by the Si interparticle spacing (approximately 10 μm spacing between the bands of high particle density). The strain gradient plasticity theory thus predicts an increased density of geometrical dislocations of the order of 2 x $10^{14}/m^2$ – for the composite material over those generated in the monolithic materials. This high density of dislocations, distributed between the individual Si particles and between the particle-rich bands, is clearly a strong driving force for more rapid substructure generation, and for continued structural refinement with increased strain.

Mechanical properties:
Following the earlier discussion of the microstructure created by severe plastic deformation, it is clear that the materials examined can be treated as fine-grained materials composed of elongated subgrain/grain structures with a high density of internal, near-randomly distributed dislocations – for materials previously strained to high levels of strain. Strengthening can therefore be analysed using the combined hardening contributions of grain boundaries, by a Hall-Petch approach, and of dislocations, by a Taylor approach. For materials strained by only a few ECAP passes the microstructure is less well defined and it is not clear how to characterise distributions of grains, subgrains or cells. At the same time as the deformation substructure refines, the Si particles refine in size, but remain very coarse and widely-separated and do not become important dislocation obstacles for significant hardening (for example using an Orowan approach).

For the as-cast Al-7%Si composite, a possible way of analysing strengthening is through the use of a rule-of-mixtures approach, treating the material as a composite with hard, undeformable particles in a soft matrix. This approach seems reasonable since there is a relatively large volume fraction (9%) of strong, needle-plate-shaped particles, see Fig. 1e. Hence, for the cast composite we can write:

$$\sigma_{0.2} = (1\text{-}f_{vp})\ \sigma_m + f_{vp}\ \sigma_p \qquad \text{(i)}$$

where $\sigma_{0.2}$ is the yield strength of the composite, $(1\text{-}f_{vp})$ and f_{vp} are the volume fraction of the matrix and particulate phase respectively, and σ_m and σ_p are the stress carried by the matrix and particulate at composite yielding. When the hard and stiff particulate are well-adhered to the matrix and do not deform plastically or fracture, yielding of the composite occurs as the matrix deforms plastically with the particulate forcing the surrounding matrix to deform more extensively locally. Load transfer to the particulate phase will be affected by factors such as the difference of elastic moduli at the interface [27] and local changes of matrix

microstructure [28]. Accordingly, the yield stress of the as-cast Al-7%Si composite can be described from equ. (i) as:

$$\sigma_{0.2} = 90 = 0.91\ (50 + \sigma_{th}) + 0.09\ (\sigma_{tr}) \qquad \text{(ii)}$$

where 90 (MPa) is the yield stress of the composite and 50 (MPa) the yield stress of the matrix (using data for the cast Al-0.5%Si, see Tables 1 and 2). σ_{th} is the matrix hardening due to thermal expansion misfit of the particles in the matrix and the dislocations generated during cooling after solidification; σ_{tr} is the stress transferred to the 9 vol % Si particulate. The Arsenault-Shi model [29] may be used to estimate the dislocation density induced during the final stages of cooling after solidification, depending on the temperature range over which thermal strains are accumulated and the difference of thermal expansion coefficients of matrix and particulate [30, 31], and the strengthening contribution of these dislocations estimated [e.g. 25, 32] using the Taylor equation with reasonable values for matrix parameters (shear modulus, Burgers vector): a value of about 20 MPa is deduced. From equ. (ii) we deduce a stress transfer to the Si particles in the cast material of about 240 MPa, somewhat larger than the flow stress of the composite itself.

For the Al-7%Si composite after severe plastic deformation, we prefer to use no longer the composite approach to analyse strengthening since the volume fraction of particulate (9%) is now present as fine and distributed equiaxed particles. As clearly shown by Boa et al [33] the strengthening achieved due to matrix-particulate incompatibility is negligible for such a microstructure. Since the dislocation hardening due to the distributed Si particles is very small (only a few MPa according to the Orowan equation), we can describe the material strength ($\sigma_{0.2}$) in terms of the matrix with its high dislocation density and fine grain size, as:

$$\sigma_{0.2} = \sigma_0 + \sigma_\rho + k/\sqrt{D} \qquad \text{(iii)}$$

the sum of an undeformed matrix term (σ_0), a dislocation hardening term (σ_ρ), and a Hall-Petch term depending on the grain size D. Fig. 12 shows the Hall-Petch interpretation of the yield stress of the Al-7%Si composite. The Hall-Petch line shown for the composite material is determined from material deformed through the whole range from 1 pass up to 10 passes, but shows no change of slope between the more lightly deformed materials (1-2 passes) and the very heavily deformed materials, where the structure can reasonably be characterized by fine subgrains/grains with a high internal dislocation density. On the same plot are shown the yield stress data for the monolothic Al-0.5%Si material after processing by ECAP, where an identical Hall-Petch slope (within experimental error) is obtained, but a much lower intercept stress value. It may be recalled at this point that the data scatter on stress values was extremely small, about the size of the symbols used in Fig. 12, while the determination of a representative grain size is difficult due to the dispersion of experimental data, as shown in the histograms of Fig. 4. From such histograms it is clear that grain sizes varied within a given material and state by more than a factor of 2 around the median grain size value used in Fig.

12. At the same time, however, the very small scatter of data points about the straight lines shown in Fig. 12 lend support to the statement that the lines are parallel, with the same Hall-Petch slope, of value 50-52 MPa $\sqrt{\mu m}$, for both materials. The two lines shown have different intercept stresses, of 52 MPa for the monolithic Al-0.5%Si alloy and 125 MPa for the Al-7%Si composite. The Hall-Petch slope is consistent with literature values for pure Al or lightly-alloyed Al, about 40-60 MPa $\sqrt{\mu m}$ [34-36], while the intercept stresses are larger than the measured yield stress of as-cast Al-0.5%Si (50 MPa, Table 2). As indicated in equ. (iii) the intercept value can be larger than the undeformed material stress due to the presence of dislocations inside the subgrains/grains, which produce Taylor hardening. The increased values of intercept stress in Fig. 12 are consistent with hardening by a high dislocation density for the composite matrix (about 1-2 x $10^{14}/m^2$) and a few dislocations for the monolithic alloy (about $10^{11}/m^2$). A high dislocation density was indeed noted inside the grains of the matrix of the deformed composite (about $10^{14}/m^2$ was estimated, see Fig. 7), and this value is similar to the number of geometrically necessary dislocations expected from the strain gradient plasticity theory. A lower dislocation density was noted inside grains of deformed monolithic Al-0.5%Si alloy (about $10^{12}/m^2$ was estimated, see Fig. 7): while this number is larger than that deduced from the intercept stress value, it should be remembered that the similarity in stress levels of intercept and experimental as-cast material, together with imprecision of precise Hall-Petch slope values, makes this analysis subject to some uncertainty.

In summary, the experimental strength of the highly deformed monolithic material is seen to be well explained by an intercept stress corresponding to that of undeformed matrix with some solute strengthening and a small dislocation hardening term, with significant grain boundary hardening described by a Hall-Petch expression. Strength of the composite is described almost completely by the behaviour of the matrix, with the dispersed, coarse particulate contributing only a very small amount to the overall composite strength. The strength of this deformed composite has three important contributions – the undeformed-solute strengthened matrix term, significant hardening by the high density of dislocations inside the grains, and significant hardening by the extremely fine grain sizes achieved in the composite. The dislocation hardening contribution appears to be approximately constant for all high levels of imposed strain, qualitatively consistent with the TEM observations. The strength of the as-cast composite is analysed through a rule-of-mixtures approach with some load transfer to the coarse particulate network, a matrix-solute term, essentially no grain size hardening term, and some hardening due to the thermally-induced dislocations.

Severe plastic defomation of the Al-7%Si composite leads not only to an increase in yield stress of a factor of three, but also an increase in ductility of three, from 4.5% to 13%, as illustrated in Fig. 8. The ductility increase is, in addition, accompanied by a significant loss of

work hardening ability, as is commonly observed for such severely deformed materials [6,11], which usually leads to some loss of ductility (seen for the heavily deformed monolithic materials in the present study). The reason for this ductility increase was the avoidance of premature brittle fracture, as occurred in the coarse-grained, as-cast composite with its very coarse Si particles. As seen in Fig. 1e and Table 1, while the average size of the Si particles was 4 μm in the as-cast materials, some Si flakes, arranged in the cellular network, reached sizes above 20μm. Such coarse flakes were easy crack nucleation and propagation sites. These flakes were broken into equiaxed blocks of size 1-2 μm by severe plastic deformation with no significantly larger Si particles. Such refinement of Si particles was a major reason for the increased ductility of the composite material, but at the same time the fracture surface observed after severe plastic deformation, Fig. 10, showed a fine dimple appearance for the Al matrix, giving the impression of this being a healthier matrix than for the as-cast state.

Conclusions

The effect of severe plastic deformation by ECAP on microstructure evolution and changes of mechanical properties has been examined on an Al-7%Si composite alloy, and compared with changes occurring in an Al-0.5%Si monolithic alloy having the same chemical composition as the matrix of the Al-7%Si composite.

The initial dendritic structure of large Al dendrites and Si particles showed an inhomogeneous cell/subgrain/microband structure after deformation to relatively low strain levels, and was transformed at a high level of strain (above about 2) into a fine-grained structure consisting of elongated submicron grains/subgrains with a high density of dislocations inside the grains and a banded distribution of finer Si particles. The microstructure of the Al-7%Si composite was much finer, and the grains contained a higher dislocation density, than the Al-0.5%Si monolithic alloy, due to the strain incompatibilty between the soft Al matrix and the hard Si particles.

Hardening during the first ECAP passes was due mainly to the introduction of the inhomogeneous and poorly-formed dislocation structures and was much greater in the Al-7%Si composite due to the many geometrically-necessary dislocations formed as a result of strain incompatibilty between the soft Al matrix and the hard Si particles. For high levels of strain, the composite remained much stronger than the monolithic Al-0.5%Si alloy due to the much finer grain size established in the composite and the higher density of retained dislocations.

The composite showed a significant increase in ductility as a result of severe plastic deformation, despite the loss of work hardening abilility typical of materials in such states,

and is shown to be due to the break-up of the initial coarse Si particles and flakes into a finer equiaxed dispersion, and also the refinement of the matrix grain structure.

Acknowledgements

We should like to acknowledge financial support of the Spanish Ministry of Education and Science under project number MAT2003-01540, as well as the award of a Juan de la Cierva post-doctoral fellowship for one of the authors (I.G.)

References

[1] Makhlouf MM, Guthy HV. J Light Met 2001;1:199.
[2] Segal VM. Mater Sci Eng A 1995;197:157.
[3] Wang J, Iwahashi Y, Horita Z, Furukawa M, Remoto M, Valiev RZ, Langdon TG. Acta Mater 1996;44:2973.
[4] Iwahashi Y, Horita Z, Remoto M, Langdon TG. Metall Mater Trans A 1998;29:2503.
[5] Valiev RZ, Islamgaliev RK, Alexandrov IV. Prog Mater Sci 2000;45:103.
[6] Hayes JS, Keyte R, Prangnell PB. Mater. Sci. Tech. 2000; 16: 1259.
[7] Morris DG, Muñoz-Morris MA. Acta Mater 2002;50:4047.
[8] Kim JC, Nishida Y, Arima H, Ando T. Mater Lett 2003;57:1689.
[9] Segal VM. Mater Sci Eng A 2004;386:269.
[10] Sun PL, Kao PW, Chang CP. Scripta Mater 2004;51:565.
[11] Gutierrez-Urrutia I, Muñoz-Morris MA, Morris DG. Mater Sci Eng A 2005;394:399.
[12] Sabirov I, Kolednik O, Valiev RZ, Pippan R. Acta Mater 2005;53: 4919.
[13] Gutierrez-Urrutia I, Muñoz-Morris MA, Morris DG. J Mater Res 2006; 21: 329.
[14] Oh-ishi K, Hasi Y, Sadakata A, Kaneko K, Horita Z, Langdon TG. Mater. Sci. Forum 2002; 396-402: 333.
[15] Xu C, Furukawa M, Horita Z, Langdon TG. Acta Mater. 2003; 51: 6139.
[16] Straumal BB, Baretzky B, Mazilkin AA, Phillipp F, Kogtenkova OA, Volkov MN, Valiev RZ. Acta Mater. 2004; 52: 4469.
[17] Apps PJ, Bowen JR, Prangnell PB. Acta Mater 2003;51:2811.
[18] Humphreys FJ. Acta Metall. 1979; 27: 1801.
[19] Humphreys FJ, Hatherly M. Recrystallization and related annealing phenomena, Pergamon, UK (1995).
[20] Ma A, Suzuki K, Nishida Y, Saito N, Shigematsu I, Takagi M, Iwata H, Watazu A, Imura T. Acta Mater 2005; 53: 211.
[21] Ma A, Suzuki K, Saito N, Nishida Y, Takagi M, Shigematsu I, Iwata H. Mater Sci Eng 2005; 399A: 181.

[22] Ma A, Takagi M, Saito N, Iwata H, Nishida Y, Suzuki K, Shigematsu I. Mater Sci Eng 2005; 408[a]: 147.
[23] Zhang Z, Hosoda S, Kim I-S, Watanabe Y. Mater Sci Eng 2006; 425A: 55.
[24] Bay B, Hansen N, Hughes DA, Kuhlmann-Wilsdorf D. Acta Metall Mater 1992; 40: 205.
[25] Hansen N, Huang X, Hughes DA. Mater Sci Eng 2001; 317A: 3.
[26] Fleck NA, Muller GM, Ashby MF, Hutchinson JW. Acta Metall Mater 1994; 42: 475.
[27] Kouzeli M, Mortensen A. Acta Mater 2002 ; 50 : 39.
[28] Arsenault RJ. Acta Metall 1991; 39: 47.
[29] Arsenault RJ, Shi N. Mater Sci Eng 1986; 81A: 175.
[30] Gray DE. editor. American Institute of Physics Handbook. New York: McGraw-Hill; 1972.
[31] Roberts RB. J Phys D: Appl Phys 1981; 14: L163.
[32] Hansen N. Trans Metal Soc AIME 1969; 245: 2061.
[33] Bao G, Hutchinson J.W. McMeeking R.M. Acta Metall Mater 1991; 39: 1871.
[34] Carreker RP, Hibberd WR. Trans AIME 1957; 209, 1157.
[35] Hansen N. Acta Metall 1977; 25: 863.
[36] Amstrong RW, Douthwaite M. In: Otooni MA et al., editors. Mater. Res. Soc. Symp. Proc. Mater. Res. Soc., vol. 362, Pittsburgh, USA;1995, p.41.

Table 1. Evolution of Grain size, Particle size and Yield stress of Al-7%Si alloy during severe deformation by ECAP

Nº ECAP Passes	**Grain size w /l (nm)**		**Si-particle size (μm)**	**$\sigma_{0.2}$ (MPa)**
(as-cast)	500μm		4	90± 5
1	420	800-1500	3.3	202 ± 2
2	320	800	2.9	217 ±3
3	250	650	--	225 ± 2
4	230	580	2.4	230 ± 5
6	210	530	--	241 ± 3
8	190	520	2.2	243 ± 3
10	170	420	1.4	245 ± 4

Table2. Evolution of Grain size and Yield stress of the single phase Al and Al-0.5%Si alloys during severe deformation by ECAP

	Alloy Al-0.5%Si		**Single phase Al**	
Nº ECAP Passes/Strain	**Grain size w / l (nm)**	**$\sigma_{0.2}$ (MPa)**	**Grain size w / l (nm)**	**$\sigma_{0.2}$ (MPa)**
(as-cast)	500μm	50± 2	500μm	45± 3
1 / 0.7	780 / 800-2000	104 ± 4	----	96 ± 4
3 / 2.1	530 / 1200	123 ± 3		
4 / 2.8	340 / 820	137 ± 5	350 / 720	130 ± 5
8 / 5.6	300 / 720	146 ± 1	310 / 700	143 ± 5
10 / 7	290 / 680	148 ± 1		

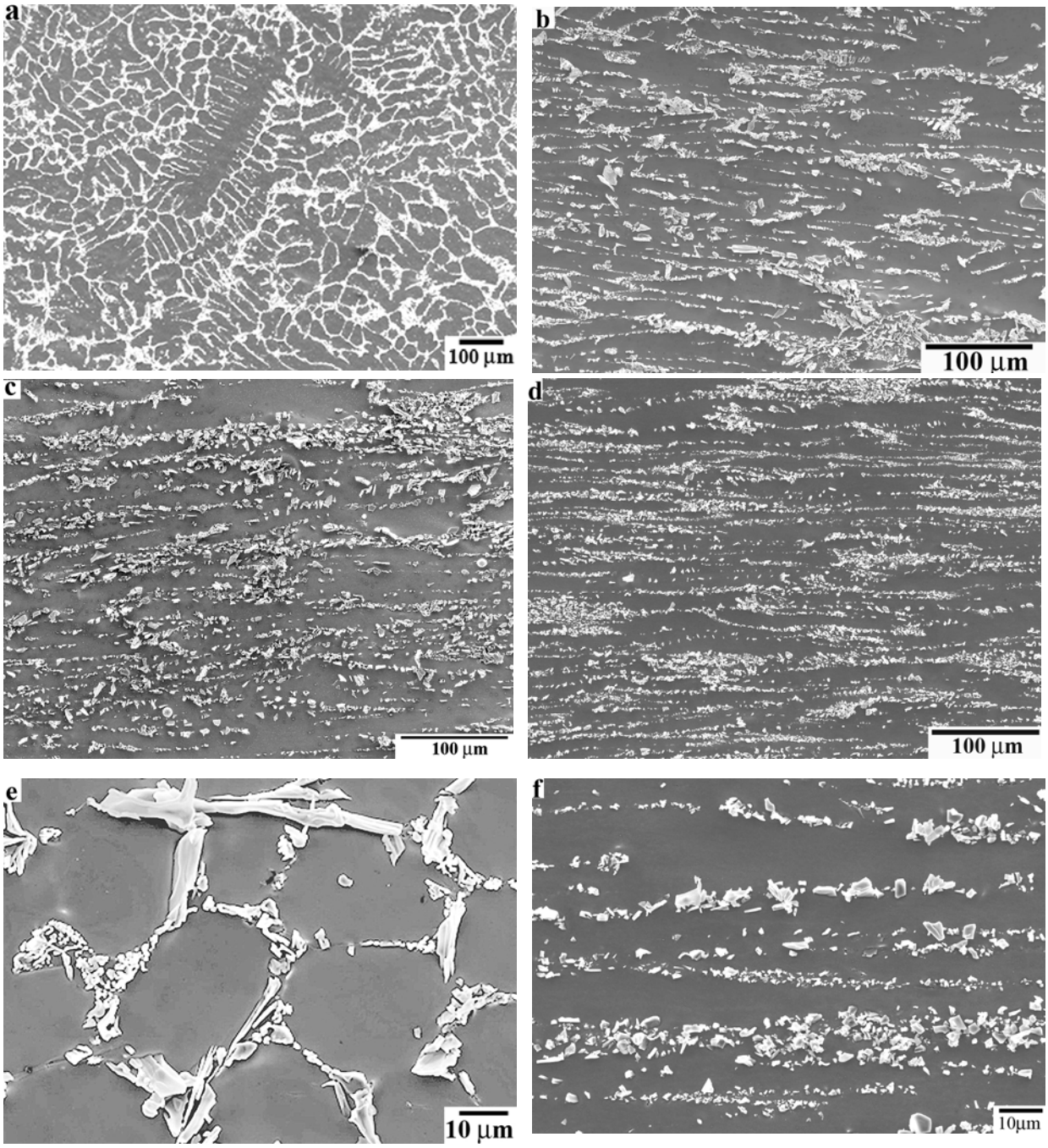

Fig. 1. Effect of severe deformation on interdendritic networks of Si particles. (a) as-cast material; (b) after two ECAP passes, (c) four ECAP passes, and (d) 10 ECAP passes. Details of Si particle distribution in as-cast state (e) and after ten ECAP passes (f).

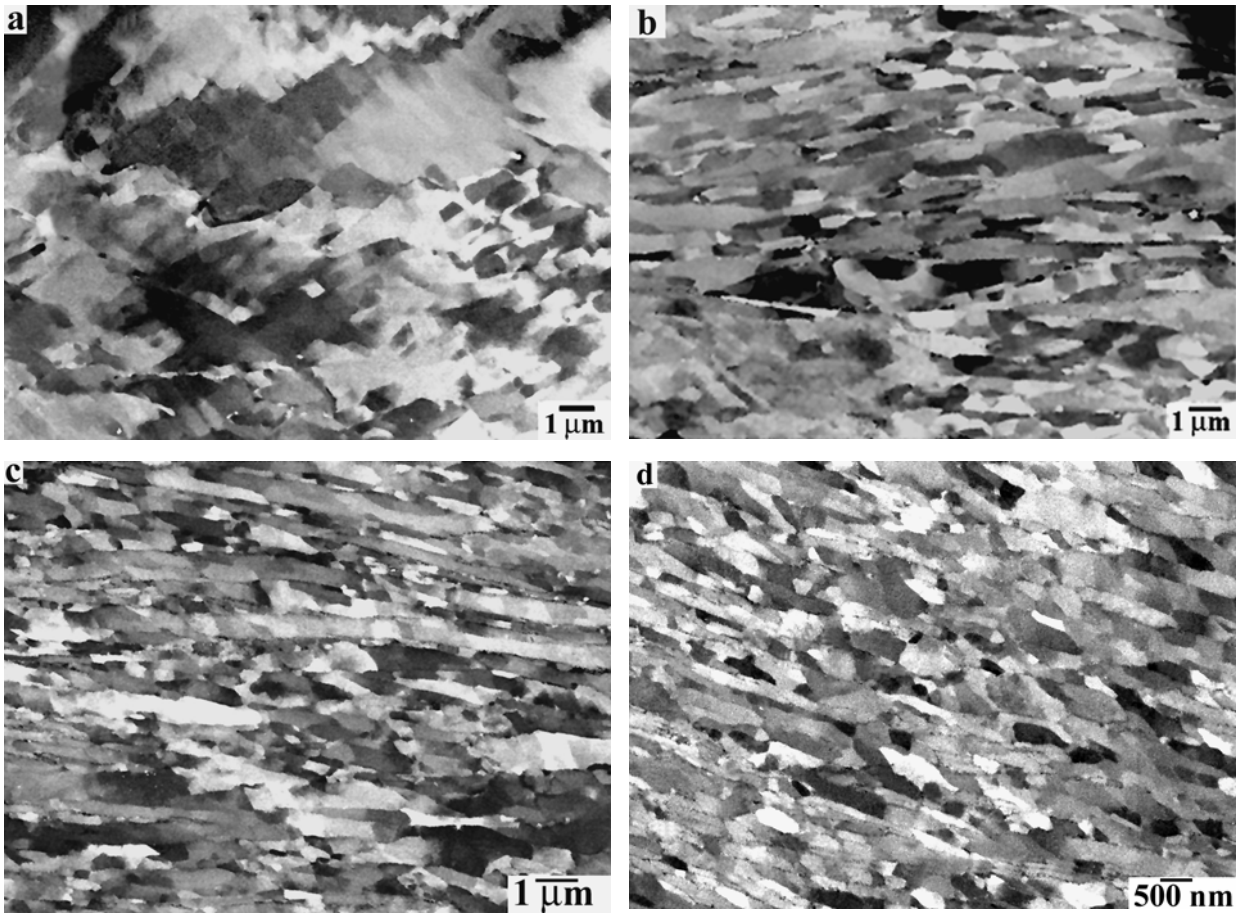

Fig. 2. Back scattered electron images in SEM of subgrain/ grain microstructures produced by severe deformation of Al-7Si alloy after one ECAP pass (a), four ECAP passes (b), eight ECAP passes (c) and ten ECAP passes (d).

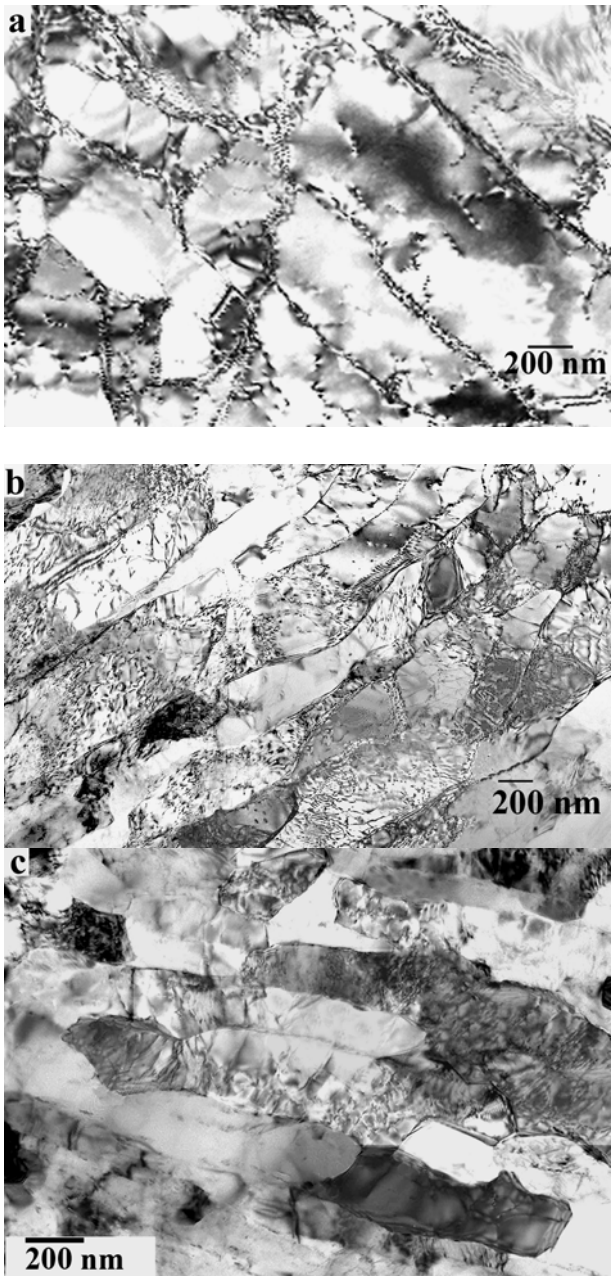

Fig. 3. TEM images of subgrain/ grain microstructures produced by severe deformation of Al-7Si alloy after one ECAP pass (a), four ECAP passes (b) and ten ECAP passes (c).

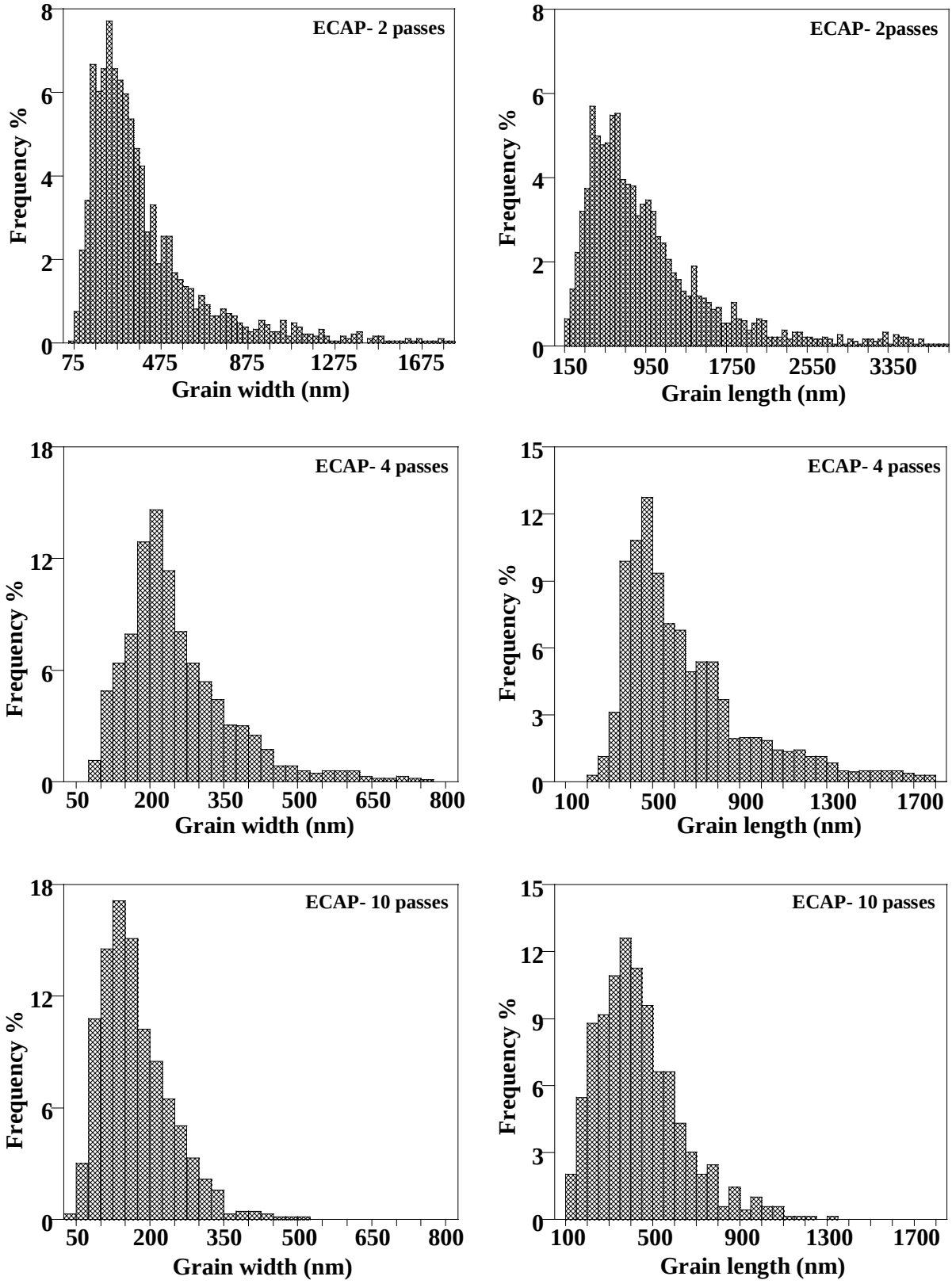

Fig.4. Examples of histograms obtained from quantitative measurements of grain size in Al-7Si alloy (width and length) after two, four and ten ECAP passes.

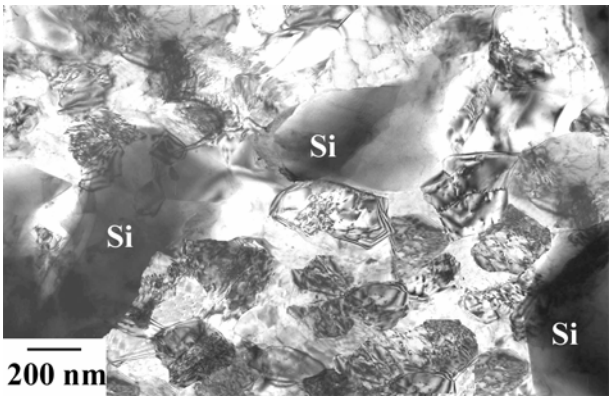

Fig.5. Bright field TEM micrograph showing equiaxed grains produced by severe deformation after eight ECAP passes in zones adjacent to large Si particles.

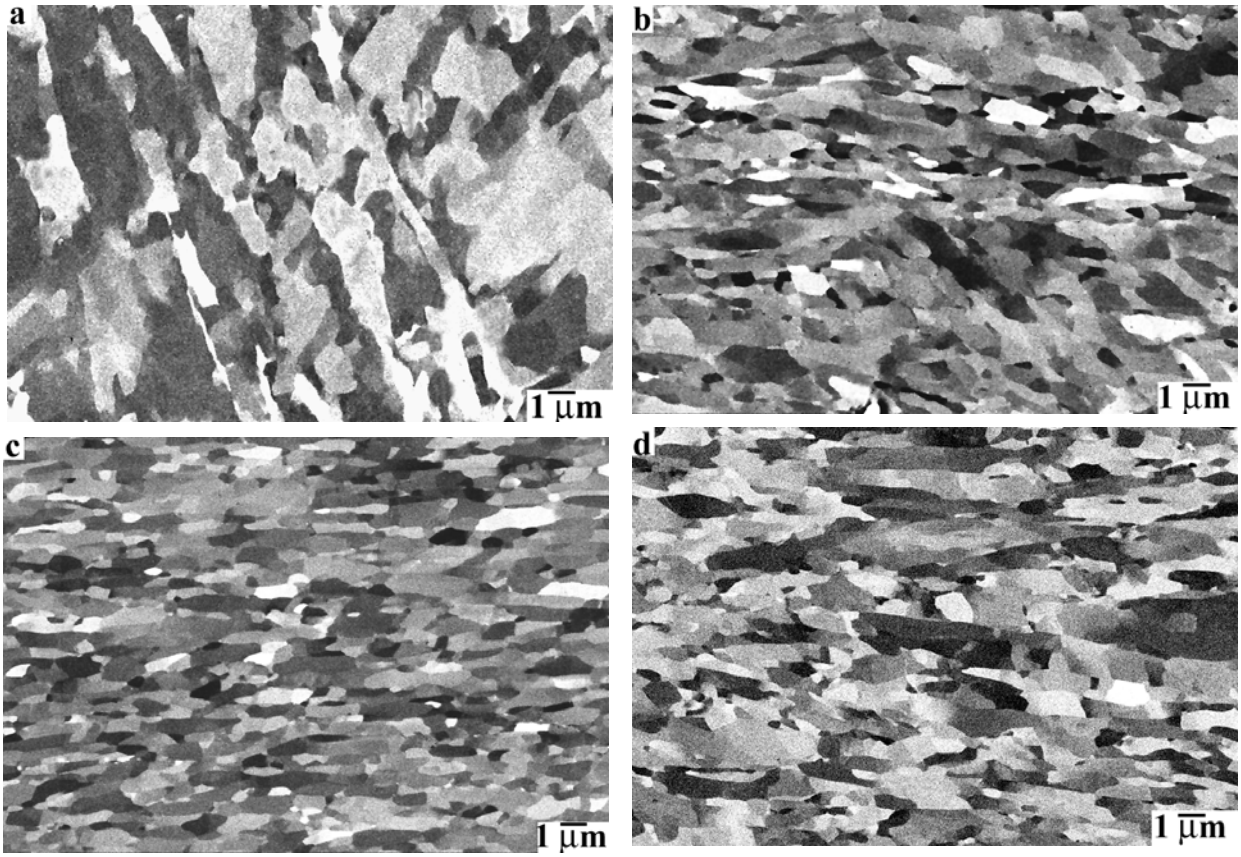

Fig.6. Back scattered electron images in SEM of subgrain/ grain microstructures produced by severe deformation of Al-0.5% Si alloy after one (a), four (b) and eight (c) ECAP passes.Also shown is an equivalent grain structure in Al after eight ECAP passes (d).

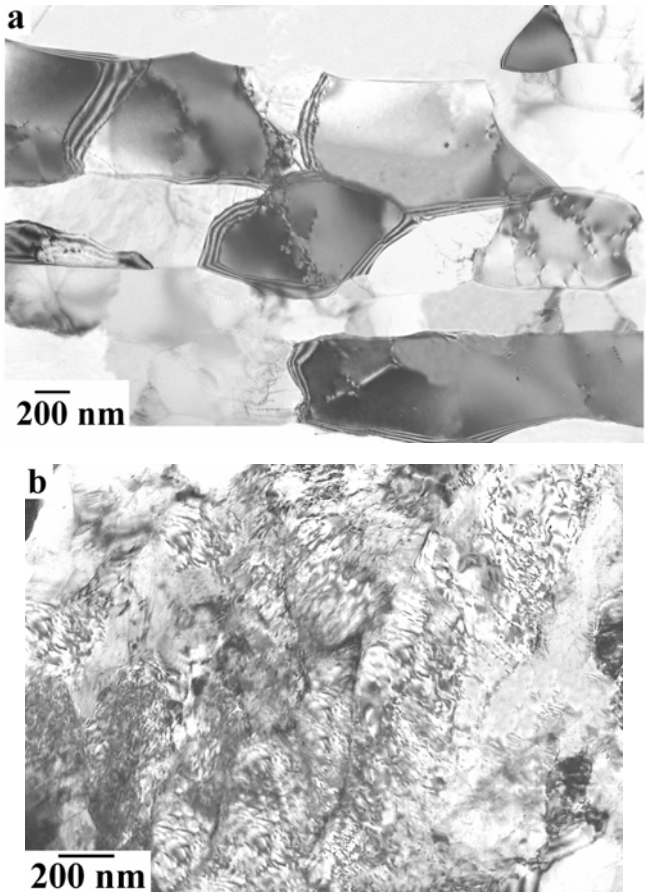

Fig.7. Bright field TEM micrographs showing differences of grain size and dislocation density inside the grains after deforming to eight ECAP passes: (a) Al-0.5%Si, (b) Al-7%Si.

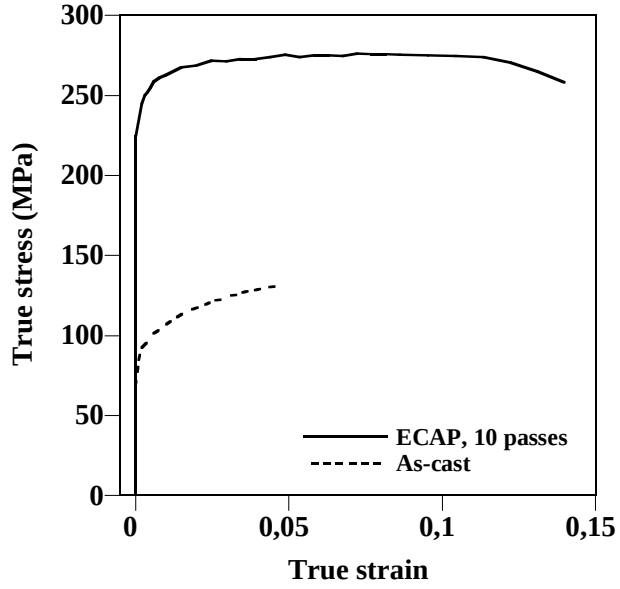

Fig.8: Examples of true stress-true strain curves obtained from tensile tests of the Al-7%Si alloy in the as-cast state and after processing by ten ECAP passes.

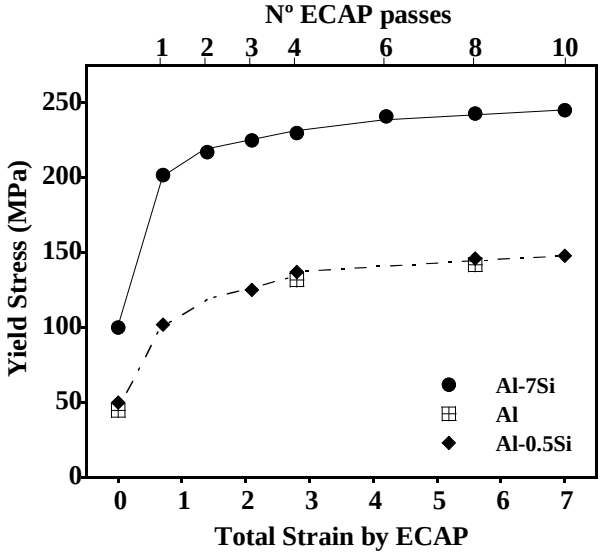

Fig.9. Yield stress evolution as a function of the total strain achieved during processing by ECAP in the Al-7% Si alloy and Al-0.5%Si and Al used as reference materials.

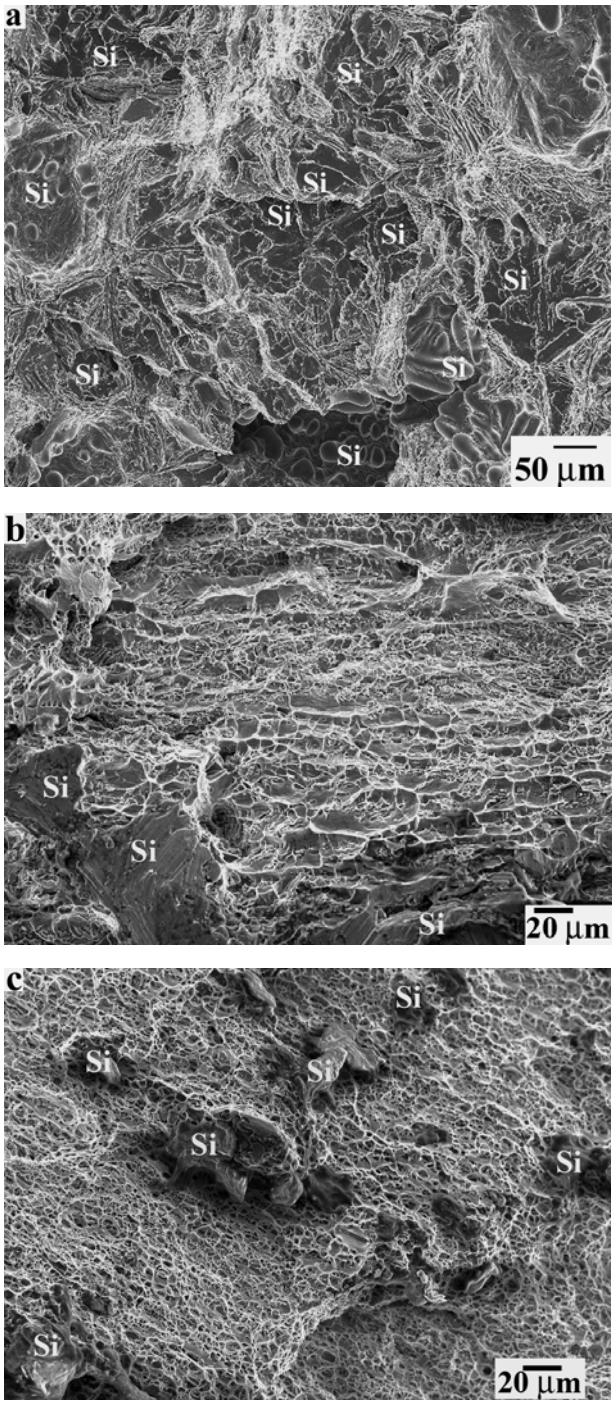

Fig. 10. SEM images of fracture surfaces tensile tested Al-7%Si alloy in the as-cast state (a) and after severe deformation processing by ECAP to total strains of (b) 1.4 and (c) 7.

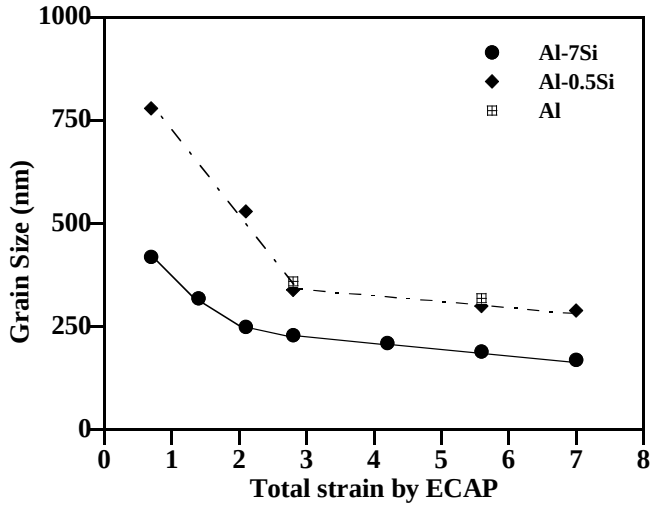

Fig. 11. Evolution of grain size with total strain imposed by ECAP for the Al-7%Si composite and the monolithic Al-0.5%Si and Al materials.

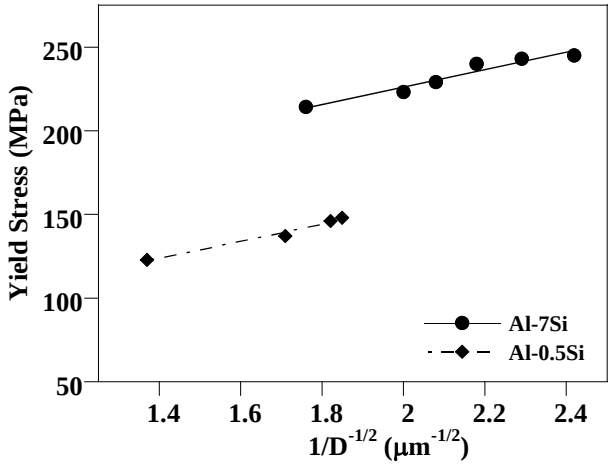

Fig. 12. Hall-Petch plot relating flow stress to reciprocal square root of grain size for the monolithic Al-0.5%Si and the Al-7%Si composite.